Retrospective Assessment of Deep Neural Networks for Skin Tumor Diagnosis

Seung Seog Han, MD[1], Ik Jun Moon, MD[1], Jung-Im Na MD, Myoung Shin Kim, MD, Gyeong Hun Park, MD,

Seong Hwan Kim, MD, Kiwon Kim, MD, Ju Hee Lee, MD[*], Sung Eun Chang, MD[*]

Author Affiliations
Department of Dermatology, I Dermatology Clinic, Seoul, Korea (Han);
Department of Dermatology, Severance Hospital, Yonsei University College of Medicine, Seoul, Korea (Moon, Lee)
Department of Dermatology, Seoul National University Bundang Hospital, Seongnam, Korea (Na);
Department of Dermatology, Sanggye Paik Hospital, Inje University College of Medicine, Seoul, Korea (Kim MS);
Department of Dermatology, Dongtan Sacred Heart Hospital, Hallym University College of Medicine, Seoul, Korea (Park);
Department of Plastic and Reconstructive Surgery, Kangnam Sacred Hospital, Hallym University College of Medicine, Seoul, Korea (Kim SH);
Department of Rehabilitation Medicine, Seoul National University College of Medicine, Seoul, Korea (Kim KW);
Department of Dermatology, Asan Medical Center, Ulsan University College of Medicine, Seoul, Korea (Chang);

[1]These authors contributed equally to this work.

*Correspondence

#1 Sung Eun Chang, MD, #2 Ju Hee Lee, MD

*Correspondence #1 : Sung Eun Chang
Email: csesnumd@gmail.com
Address: Department of Dermatology, Asan Medical Center, Ulsan University College of Medicine, 88, OLYMPIC-RO 43-GIL Songpa-gu, Seoul, 05505, Korea
Fax: +82-2-486-7831
Phone: +82-2-3010-3460

*Correspondence #2 : Ju Hee Lee
Email: juhee@yuhs.ac
Address: Department of Dermatology, Severance Hospital, Yonsei University College of Medicine,50-1 Yonsei Ro, Seodaemun-gu Seoul, 03722, Korea
Fax: +82-2-393-9157
Phone: +82-2-2228-2080

Abbreviations:
AUC, area under the curve; CNN, convolutional neural network; PPV, positive predictive value; ROC curve, receiver operating characteristic curve; RCNN, region-based convolutional neural network; NPV, negative predictive value

ABSTRACT

BACKGROUND

The aim of this study was to validate the performance of algorithm (http://rcnn.modelderm.com) for the diagnosis of benign and malignant skin tumors.

METHODS

With external validation dataset (43 disorders; 40,331 clinical images from 10,426 patients; January 1, 2008 – March 31, 2019), we compared the prediction of algorithm with the clinical diagnosis of 65 attending physicians at the time of biopsy request.

RESULTS

For binary-task classification of determining malignancy, the AUC of the algorithm was 0.863(95% CI 0.852–0.875) with unprocessed clinical photographs. The sensitivity/specificity of the algorithm at the predefined high-sensitivity and high-specificity threshold were 79.1%(76.9–81.4)/76.9%(76.1–77.8) and 62.7%(59.9–65.5)/90.0%(89.4–90.6), respectively. The sensitivity/specificity calculated by the clinical diagnosis of attending physicians were 88.1%/83.8%(Top-3) and 70.2%/95.6%(Top-1), which were superior to those of algorithm.

For multi-task classification, the mean Top-1,2,3 accuracies of the algorithm were 42.6±20.7%, 56.1±22.8%, 61.9±22.9%, and those of clinical diagnosis were 65.4±17.7%, 73.9±16.6%, 74.7±16.6%, respectively.

CONCLUSIONS

The performance of the algorithm was lower than that of dermatologists in real practice. To expand data relevancy, not only image information, but also clinical information should be integrated for more accurate prediction.

Introduction

Deep learning algorithm has shown excellent results in analyzing fundoscopy images in ophthalmology[1], chest X-ray[2] and CT images in radiology.[3] In dermatology, there have been remarkable advances that showed results comparable to dermatologists' diagnostic performance using both clinical photography[4-9] and dermoscopy images.[4,7,10-13]

However, it is unclear that these excellent results can be extrapolated in clinical setting as like product in other field[14]. On perspective of data relevancy, DeepMind's AlphaGo[15] was trained with Go data which had 100% data relevancy, and surpassed human champion. In speech recognition, gestures may be helpful in understanding conversation completely, but audio data shows data relevancy close to 100%. However, in medical field, clinical data used in training has relatively low data relevancy. For example, even if algorithm will be trained with countless brain MRIs, we cannot clearly answer whether the algorithm can truly diagnose Parkinson's disease with MRI alone. Although image of skin contains important relevant information, there is no study of how much important in skin cancer diagnosis. This study was designed to compare the performance of algorithm with that of attending physician in real practice for the diagnosis of benign and malignant tumors.

In addition, deep learning algorithm can produce reliable result only for the preselected diseases because algorithm may show epistemic uncertainty for untrained problems[16]. Because most of previous studies had a limitation that small number of disorders were validated[17], we investigated the generalizability of our algorithm with almost all sorts of skin tumors.

Methods

With approvals of institutional review boards (Severance: #2019-0571 and Asan: #2017-0087), we gathered clinical photographs from Severance Hospital, Department of Dermatology, collected from January 1, 2008 to March 31, 2019. Attending physicians had recorded the clinical diagnosis on the biopsy request form considering patient's history and physical examinations. All skin lesions of patients over 19 years of age who were pathologically diagnosed among 43 primary skin tumors were included (Figure 1). We included cases with

single lesion because of the possible mismatch between the lesion and the diagnosis for patients with multiple lesions. We excluded the images of intraocular, postoperative, laser surgery, and other chief complaints, but we did not exclude normal images taken for record taking even if it did not include the lesion of interest. There were 66 cases with inadequate quality and 769 cases with which it was inherently impossible to detect lesions (Figure 1). As a result, a total of 40,331 clinical images from 10,426 patients were included in this study (Table 1).

THE ALGORITHM

To validate the generalizability, the algorithm created in the previous study was tested again without modification in this study. The algorithm was trained not only with hospital archives but also with the archives generated with assistance of region-based convolutional neural network (RCNN) to reduce false positives. As a result, the algorithm was trained with 1,106,886 image crops. Algorithm has two parts: (A) lesion detection part and (B) disease classifier part. The lesion detection part was trained with faster RCNN (backbone=VGG-16) and CNN (SE-ResNet-50). The disease-classifier part was trained with CNNs (SENet and SE-ResNeXt-50).
The web-DEMO of the algorithm has been available in public (http://rcnn.modelderm.com) to facilitate scientific communications. We used the malignancy output which was predefined as: malignancy output = (basal cell carcinoma output + squamous cell carcinoma output + intraepithelial carcinoma output + keratoacanthoma output + malignant melanoma output) + 0.2 × (actinic keratosis output + ulcer output).

PREDEFINED HIGH-SENSITIVITY THRESHOLD AND HIGH-SPECIFICITY THRESHOLD

We used two predefined thresholds (high-sensitivity threshold which was formerly named as T_{90} in the previous study and high-specificity threshold which was named as T_{80}. These cut-off thresholds were defined as 90% or 80% sensitivity points with the dataset from Asan Medical Center, Department of Dermatology. In the dataset, all patients suspected of 10 major tumorous disorders (the same tumors as those of the Edinburgh dataset) from January 1, 2018 to June 30, 2018 were serially included. After pathologic confirmation, the dataset comprised of malignant tumors (81 patients), benign tumors (251 patients), and other various benign disorders (54 patients).

UNPROCESSED IMAGE ANALYSIS VERSUS CROPPED IMAGE ANALYSIS

There are two different ways in using the algorithm for lesion diagnosis. The user or patient may localize the lesion of interest (cropped image analysis). If not, the algorithm needs to analyze unprocessed photograph without information on the lesion of interest (unprocessed image analysis). In unprocessed image analysis, our algorithm detected the lesion of interest in the photograph, and the highest malignancy output was used as the final output score among the malignancy outputs of suspected lesions. In cropped image analysis, the average malignancy output of the multiple lesions of interest was used as the final output score.

STATISTICAL ANALYSIS

We evaluated the performance of algorithm for the determination of malignancy. For the binary classification test, we draw ROC curve using the final output scores(the highest malignancy output in unprocessed image analysis and the average malignancy output in cropped image analysis) and calculated area under the curve (pROC package version, 1.15.3; R version 3.4.4). The confidence interval was computed with 2,000 stratified bootstrap replicates.

Results

BINARY CLASSIFICATION

With the Dataset A, the algorithm analyzed all photographs of each patient for determining malignancy. The AUC value for determining malignancy was 0.863(95% CI 0.852–0.875).

At predefined high-sensitivity threshold, the sensitivity/specificity was 79.1%(76.9–81.4), 76.9%(76.1–77.8), and at predefined high-specificity threshold, the sensitivity/specificity was 62.7%(59.9–65.5), 90.0%(89.4–90.6) (Table 2). The sensitivity/specificity of the clinical diagnosis for malignancy determination calculated by clinical impressions were 70.2%/95.6%(Top1) and 88.1%/83.8%(Top3) (Figure 1). The differences between Top-1 clinical diagnosis and the algorithm at high-specificity threshold and the difference between Top-3 clinical diagnosis and the algorithm at high-sensitivity were statistically significant (McNemar test; all P<0.0001).

The positive predictive value (PPV) of the algorithm were 31.3%(30.3–32.3) at high-sensitivity threshold and 45.4%(43.7–47.3) at high-specificity threshold, and the PPVs of Top-1 and 3 clinical diagnosis were 68.1%, 41.9%. The negative predictive value (NPV) of the algorithm were 96.5%(96.2–96.9) at high-sensitivity threshold and 94.8%(94.4–95.2) at high-specificity threshold, and the NPVs of Top-1 and 3 clinical diagnosis were 96.0% and 98.1%.

The performances of two analysis methods (unprocessed image analysis versus cropped image analysis) were compared with 39,721 images from 10,315 patients (Figure 3). The AUC of 0.881(0.870–0.891) in cropped image analysis was slightly better than the AUC of 0.870(0.858–0.881) in unprocessed image analysis (DeLong's test; P=0.0022).

MULTICLASS CLASSIFICATION WITH 32 SKIN TUMORS OF THE SEVERANCE DATASET

For multi-class classification test, we used AUC and Top-accuracy as evaluation metrics. We calculated both Top accuracy of total patients and Top accuracy of each classes because the number of patients varies in each classes.

The calculation of Top accuracy of each classes was performed with 32 disorders (Severance Dataset B; 39,721 images from 10,315 patients). We excluded 6 classes (angiofibroma, Café au lait macule, juvenile xanthogranuloma, milia, nevus spilus, and sebaceous hyperplasia) of which the number of patient was less than 10, and we also excluded 5 classes (Spiz nevus, dermatofibrosarcoma protuberans, angiosarcoma, Kaposi's sarcoma, and Merkel cell carcinoma) which were not trained to the algorithm. We calculated mean accuracy by averaging the accuracies of 32 disorders as follows: macro-averaged mean Top-(n) Accuracy = (Top-(n) Accuracy of actinic keratosis + Top-(n) Accuracy of angiokeratoma + … + Top-(n) Accuracy of xanthelasma) / 32. The macro-averaged mean Top-1 and 3 accuracies of clinical diagnosis were 65.4±17.7% and 74.7±16.6%, and those of the algorithm were 42.6±20.7% and 61.9±22.9%, respectively. In order to reflect the difference in the number of cases for each disease, the micro-averaged accuracy was calculated as follows : micro-averaged mean Top-(n) Accuracy = (Top-(n) matched cases in total) / 10,315. The micro-averaged mean Top-1 and 3 accuracies of clinical diagnosis were 68.2% and 78.7% and those of the algorithm were 49.2% and 71.2%, respectively.

The mean AUC of 32 classes was 0.931±0.062 (Figure 4 and Table 4).

MULTICLASS CLASSIFICATION WITH 10 SKIN TUMORS OF THE EDINBURGH DATASET

We performed an additional external validation with the Edinburgh dataset. The Edinburgh dataset consists mainly of Caucasians and is commercially available dataset with 10 benign and malignant skin tumor (Table 5; https://licensing.edinburgh-innovations.ed.ac.uk/i/software/dermofit-image-library.html). In previous studies[4,5], the Edinburgh dataset was used as a validation dataset.

For the multi-class classification, the macro-averaged mean Top-1 and 3 accuracies were 53.0% and 77.6%, respectively and the mean AUC of each classes was 0.939±0.030 (Figure 5 and Table 5).

Discussion

Deep learning algorithm has recently shown remarkable performance in dermatology. With clinical photographs[4-8] and dermoscopic images[4,7,10-13], algorithm showed comparable or superior performance to dermatologists with regards to the problem of malignant melanoma vs nevus, and carcinoma vs benign keratotic tumors. Direct comparison between the results of various studies is difficult because inclusion and exclusion criteria of validation dataset are unclear and the validation datasets were private[18]. To date, there have been only few studies that compared the algorithm's performance with experts using external datasets.[19] It was impossible to test their algorithm in most studies and it was unknown whether the algorithm could reproduce similar performance with other datasets. In fact, several studies report that currently available smartphone applications did not show the dermatologist-level performance as shown in academic papers.[20,21]

When investigating the performance of deep learning algorithm with skin diseases, there are various factors that result in poor reproducibility or generalizability in real practice.

1) Limited number of training classes: the number of disorders in validation dataset is usually much smaller than that in real practice[17]. Algorithm had shown good performance with a narrow range problem such as “melanoma vs nevus”. However, as shown in Table 4, the mean Top-1 accuracy of clinical diagnosis was only 65.4%, which suggests that it is hard to choose the initial problem correctly. For example, the algorithm trained only with melanoma and nevus may be misused for the diagnosis of other disorder such as seborrheic keratosis, which result in epistemic uncertainty.[16]

2) Innocent biases of internal validation: in internal validation, prediction may be drawn from unexpected false features instead of true features of disease. The composition of image and the presence of skin markings were likely to affect the prediction of algorithm.[22,23] From the perspective that algorithm may be trained with unexpected structured noise, the current convolutional neural network draws a statistical prediction from massive image data, rather than real intelligence.

3) Preselection of specialist: Preselection bias exists if the image is acquired in real time procedure, such as endoscopy, ultrasonography, and clinical photography. In dermatology, both training and test datasets are created by dermatologist and dermatologist determines which lesions need to be included and which composition is adequate. Because algorithm shows aleatory uncertainty, we may not get the same performance without the preselection of dermatologist.

4) Unclear inclusion and exclusion criteria: selection bias affects the result if the cases with negative results were excluded more frequently for any reason. All patients in the archives should be selected based on specific exclusion criteria to prevent selection bias.

4) Specific optimization: hyperparameters of algorithm may be specifically optimized to the validation dataset at the test time, and lack of generalizability for other dataset.

5) Data leakage: data leakage occurs when training and test dataset were not split completely, or when the data set framework is designed incorrectly. In case of data leakage, model uses inessential additional information for classification.[24]

7) Non-representativeness of training dataset[25]: hospital achieve include extraordinary case which requires biopsy. For example, there are many cases of small melanoma which does not have characteristic bizarre morphology. If algorithm was trained through these extraordinary cases, it may show many false positives. In addition, hospital achieve does not usually have enough number of images of common disorders, which reduces the diagnostic accuracy for common disorders.

8) Data relevancy: although algorithm analyze image better than dermatologist, dermatologist in real practice shows much better diagnostic accuracy because dermatologist considers all patient's information for diagnosis.

To minimize biases, this study was designed with the following considerations. 1) To prevent uncertainty for untrained classes, we included almost all kinds of skin tumors (43 disorders). 2) To avoid selection bias, all biopsied cases in one hospital were included with exclusion criteria. 3) In order to prevent innocent bias from data leakage, we tested with two external validation datasets, the Severance dataset and Edinburgh dataset. 4) To show generalizability, we verified previously created algorithm with new validation dataset built later. 5) The diagnostic accuracy of algorithm was compared with that of attending physician who considered all information of patient for diagnosis. 6) Algorithm was tested with unprocessed images without preselection of dermatologist.

To date, most comparisons between dermatologist and algorithm have been performed using single cropped image of lesions. Deep learning algorithm has shown comparable performance with dermatologists in the same settings.[4,5,7,8,11-13] Meta-analysis of medical studies also showed that, under the same conditions, the performance of algorithms was comparable to that of healthcare specialists.[19]

In this study, we investigated the diagnostic accuracy of the dermatologist in real practice with biopsied cases. Skin cancer diagnosis is a difficult task for experienced dermatologists even when given all clinical information. The sensitivity which calculated from three differential impressions of the dermatologists was 88.1%, meaning that 11.9% of malignant tumors were ignored by the dermatologists even after thorough examination, but the presence of malignancy was notified later after receiving the biopsy report. The malignancy prediction derived from the first clinical impression was 70.2%, implying that there was 29.8% misdiagnosis in the initial impression. In the multiclass classification which requires correct diagnosis, the mean Top-1 and 3 accuracy of the clinical diagnosis were lower as 65.4±17.7% and 74.7±16.6% as shown in Table 4. Deep learning algorithm

shows uncertainty for untrained task[16], therefore, if the algorithm is not an unified classifier but a classifier trained with limited classes, the precondition may be wrong[26].

The performance of attending physician significantly improves after considering various information of patient. In the actual medical practice, physician consider not only the visual information of the lesion but also various information such as previous medical history, referral note, demographics, family history, and physical examination, to improve the diagnostic accuracy. In radiology or pathology, the actual reader does not diagnose with image alone, but they also checks medical history through chart review and reflects clinicopathologic correlation. At present, there has been several reports[27-29] to reflect patient's metadata with multimodal approach. The results obtained by combining images and patient clinical information showed a general improvement of around 7% in accuracy.[27]

Algorithms may play an important role in the screening of suspected patients if mass diagnostics task will be done only with image information. Our algorithm showed a comparable performance in full automatic mode regardless of preselection of the lesion (AUC with unprocessed images = 0.870 vs AUC with cropped image = 0.881). In previous study[9] with unprocessed facial images, our algorithm showed an AUC of 0.896 with the internal validation (386 patients; 81 with malignant tumor and 305 with benign tumor) and the performance of algorithm was comparable with that of 13 dermatologists in terms of F1 score and Youden index. We reproduced a similar AUC of 0.863 with large scale external validation dataset.

Algorithm can work endlessly with minimal cost. In case of cancer screening, clinical photographs may be available alone without other information. In this study, the sensitivity at the high-sensitivity threshold was 79.1%, which was located between the sensitivities (70.2% and 84.9%) derived from the Top-2 and Top-1 clinical diagnoses. In the previous study, approximately 50% images of malignant cases could be misinterpreted to benign by general public[9]. We expect algorithm-based cancer screening helps appropriate referral to dermatology in the future.

LIMITATION

Although we obtained a mean AUC of 0.939±0.030 (Table 5) with the Edinburgh dataset (1,300 images of 10 benign and malignant tumors) which mainly consists of Caucasians, we need to test our algorithm with unprocessed clinical photographs of various race/ethnicity. With the identical image of dysplastic nevus, we should warn a high chance of melanoma for Caucasian, but may recommend close-observation for Asian because melanoma is a rare disorder in Asian. We also need to test with Asian in other regions because disease prevalence may vary from region to region even if the races are the same.

In this study, most of training and validation images were taken with adequate quality. The performance of algorithm could be affected by image quality more than that of human.[22,30] Therefore, the performance of the algorithm on the photographs taken by the public must be verified in further study.

CONCLUSION

In this study, the attending physician in real practice made more accurate diagnosis because not only image information but also clinical information was considered to make a diagnosis. Without preselection of lesion by dermatologist, our algorithm showed the AUC of 0.863, which implies unprecedented potential as a mass screening tool. More clinical information should be integrated for more accurate prediction of the algorithm in the future.

ACKNOWLEDGMENTS

Thanks to PhD, Park Jeoongsung in Qualcomm for helping to stabilize the web-DEMO.

AUTHOR CONTRIBUTIONS

Han and Moon designed experiments.

Han, Moon, Lee, Na, Kim MS, Park GH, and Kim SH prepared validation datasets.

Han, Moon, and Chang performed experiments.

Han, Moon, Park, Kim MS, Na, and Kim KW interpreted results.

Han, Moon, and Kim KW wrote the manuscript and prepared the figures.

Chang and Lee supervised the study.

Han created and managed the web-DEMO.

All authors approved the final version of the manuscript.

DATA AVAILABILITY

The images used to test the neural networks described in the manuscript are subject to privacy regulations and cannot be made available in totality. The test subset may be available upon a reasonable request and an approval of IRB of the originating university hospital.

CONFLICTS OF INTEREST

None

FUNDING

None

FIGURE LEGENDS

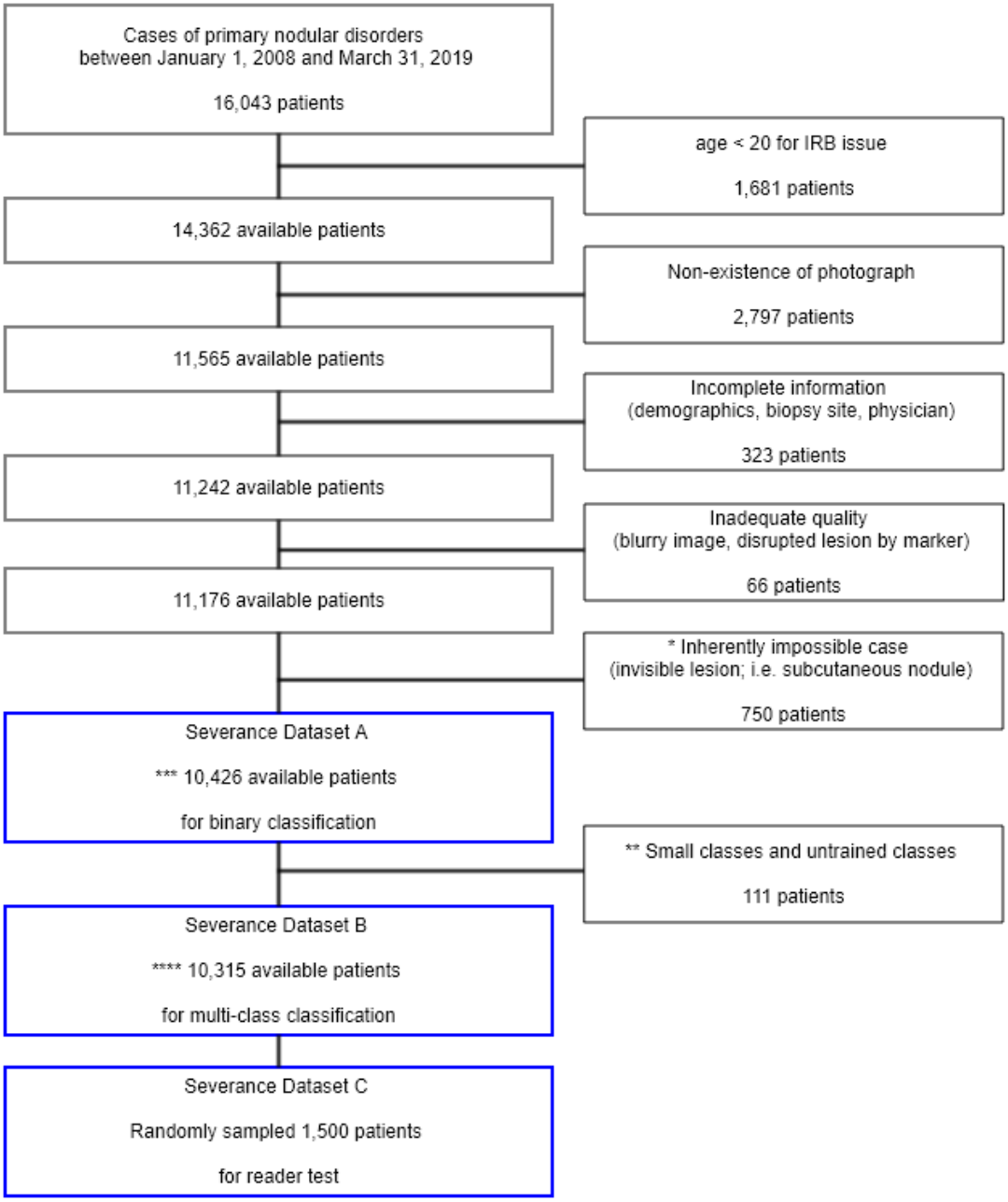

Figure 1. Dataset Selection Process - Exclusion Criteria

* The three most common disorders among the inherent impossible cases were epidermal cyst (497 cases), seborrheic keratosis (64 cases), and hemangioma (37 cases). There were 26 cases of malignant nodules (18 cases of basal cell carcinoma and 8 cases of other malignancies) among the inherent impossible cases.

** Small classes indicates the disease classes which has less than 10 cases : angiofibroma, Café au lait macule, juvenile xanthogranuloma, milia, nevus spilus, and sebaceous hyperplasia. Untrained classes indicates the classes which were not trained by the algorithm : dermatofibrosarcoma protuberans, Spitz nevus, Kaposi sarcoma, angiosarcoma, and Merkel cell carcinoma

*** Severance Dataset A; a total of 10,426 patients (40,331 images; 43 disorders; age 52.1±18.3, male 45.1%) were used for the binary-class (cancer or not) classification.

**** Severance Dataset B; a total of 10,315 patients (39,721 images; 32 disorders; age 52.1±18.2, male 44.8%) were used for the multi-class classification in the supplementary result. Among 39,721 images, a total of 34,672 images contained lesion of interests, while the remaining 5,049 images were photographs without lesion, but these photographs were taken for the purpose of observation or comparison.

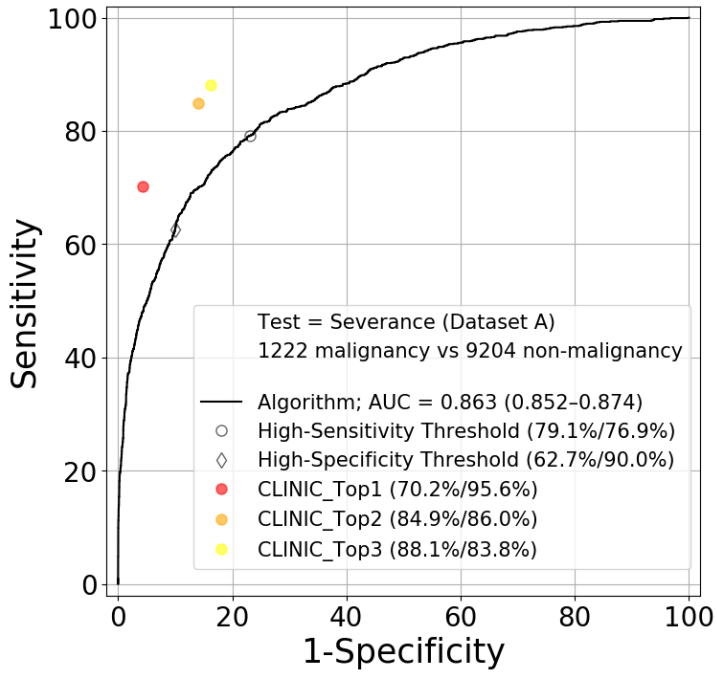

Figures 2. ROC curve of Algorithm Compared with Diagnostic Performance of the Clinical Diagnosis

Algorithm analyzed the Severance Dataset A (40,331 unprocessed images from 10,426 patients; 1,222 malignancy and 9,204 benigns).

Black curve – algorithm (unprocessed-images analysis)

Diamond – algorithm at the predefined high-sensitivity threshold

Round – algorithm at the predefined high-specificity threshold

Red, orange, and yellow circles — malignancy determination derived from Top-1, Top-2, and Top-3 clinical diagnosis of 65 attending physicians

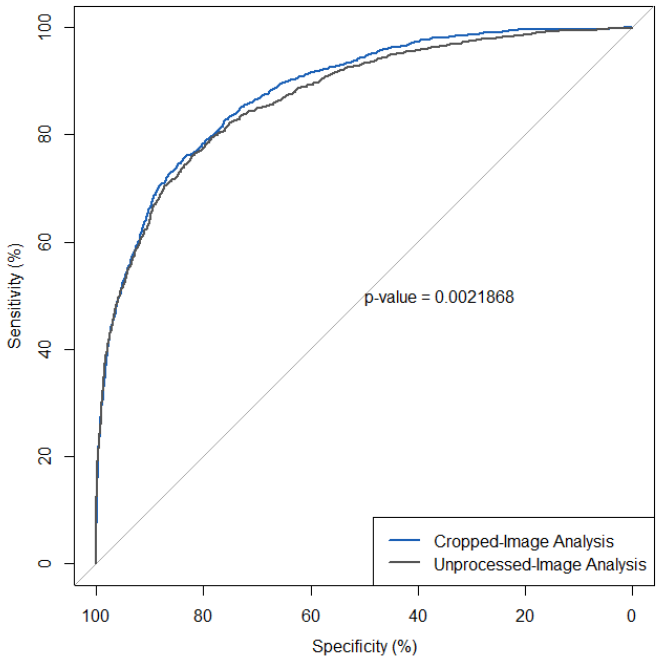

Figures 3. Performance Comparison Between Unprocessed Image Analysis and Cropped Images Analysis

Black curve – algorithm (unprocessed-image analysis)

Gray curve – algorithm (cropped-image analysis)

Severance Dataset B (39,721 images from 10,315 patients) was used for the comparison. As shown in Figure 1, the images of small classes and untrained classes were not used for this test. In cropped-image analysis, algorithm analyzed cropped lesion of interest which was pointed out by user. In unprocessed-image analysis, algorithm detected location of lesion and analyzed the suspected lesions.

The AUC in cropped-images analysis were 0.881 (95% CI 0.870–0.891), which was slightly higher than the AUC of 0.870 (95% CI 0.858–0.881) in unprocessed-image analysis.

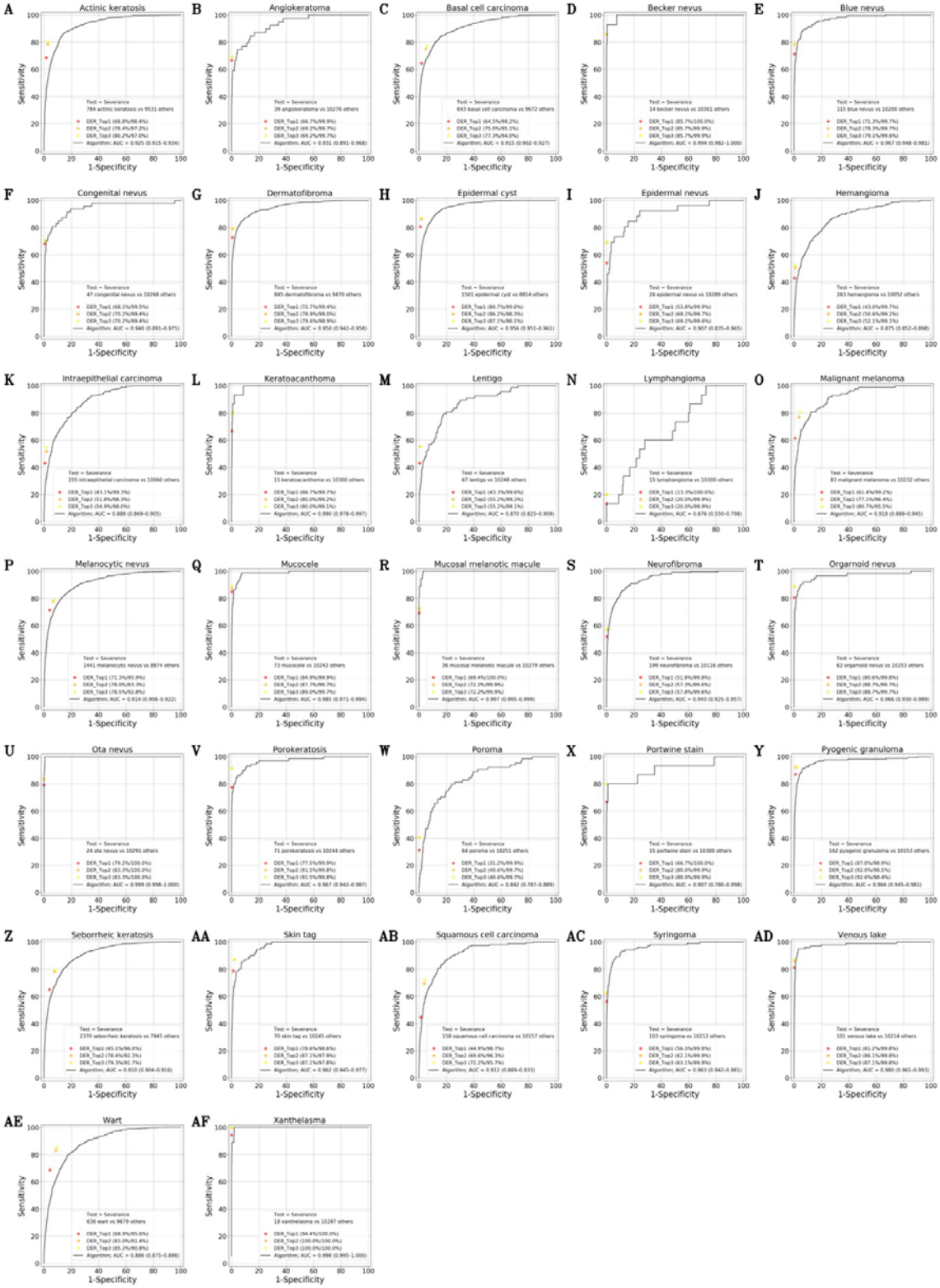
A Actinic keratosis
B Angiokeratoma
C Basal cell carcinoma
D Becker nevus
E Blue nevus
F Congenital nevus
G Dermatofibroma
H Epidermal cyst
I Epidermal nevus
J Hemangioma
K Intraepithelial carcinoma
L Keratoacanthoma
M Lentigo
N Lymphangioma
O Malignant melanoma
P Melanocytic nevus
Q Mucocele
R Mucosal melanotic macule
S Neurofibroma
T Organoid nevus
U Ota nevus
V Porokeratosis
W Poroma
X Portwine stain
Y Pyogenic granuloma
Z Seborrheic keratosis
AA Skin tag
AB Squamous cell carcinoma
AC Syringoma
AD Venous lake
AE Wart
AF Xanthelasma
Sensitivity
1-Specificity

Figure 4. Multiclass Task – The ROC of the Algorithm with 32 Skin Tumors of the Severance dataset

Algorithm analyzed the Severance Dataset B (39,721 images of 10,315 patients; 32 disorders).

The images analyzed were cropped around lesion of interest.

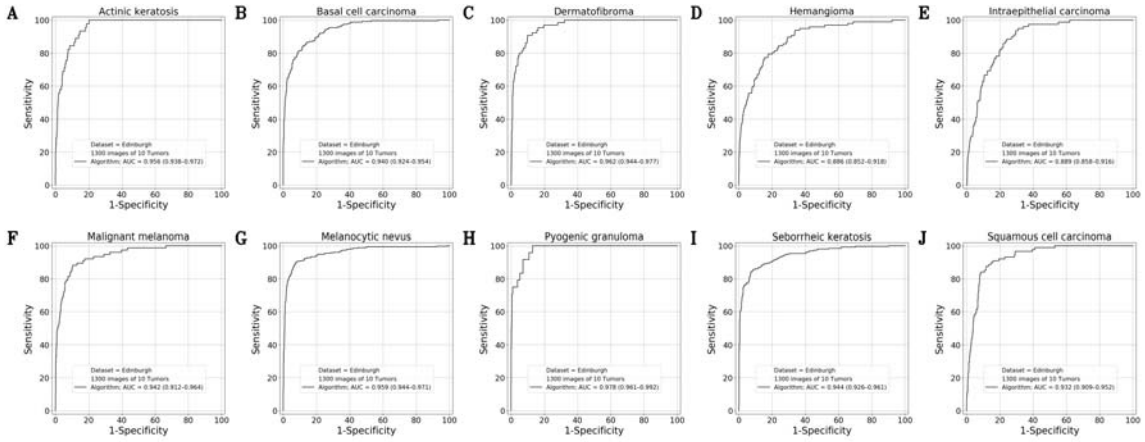

Figure 5. Multiclass Task – The ROC curve of the Algorithm with 10 Skin Tumors of the Edinburgh dataset

Algorithm analyzed 1,300 images of the Edinburgh dataset (https://licensing.edinburgh-innovations.ed.ac.uk/i/software/dermofit-image-library.html).

All the images of the Edinburgh dataset were cropped images of lesion of interest.

We draw the ROC curve in a one-versus-rest manner.

TABLES

Table 1. Demographics of the Severance Validation Dataset

	Severance Dataset	
	Dataset A	Dataset B
No. of images	40,331	39,721
Patient demographics		
No. of Patients	10,426	10,315
Age (mean ± SD)	52.1 ± 18.3	52.1 ± 18.2
Male	4,701 (45.1%)	4,626 (44.8%)
No. of disorders	43	32
Malignancy	1,222 (11.7%)	1,154 (11.2%)
Angiosarcoma	17 (0.2%)	-
Basal cell carcinoma	643 (6.3%)	643 (6.2%)
Dermatofibrosarcoma protuberance	9 (0.1%)	-
Intraepithelial carcinoma (SCC in situ)	255 (2.5%)	255 (2.5%)
Kaposi sarcoma	39 (0.4%)	-
Keratoacanthoma	15 (0.1%)	15 (0.1%)
Malignant melanoma	83 (0.8%)	83 (0.8%)
Merkel cell carcinoma	3 (0.0%)	-
Squamous cell carcinoma	158 (1.5%)	158 (1.5%)
Benign	9,204 (88.3%)	9,161 (88.8%)
Actinic keratosis	784 (7.6%)	784 (7.6%)
Angiofibroma	4 (0.0%)	-
Angiokeratoma	39 (0.4%)	39 (0.4%)
Becker nevus	14 (0.1%)	14 (0.1%)
Blue nevus	115 (1.1%)	115 (1.1%)
Café au lait macule	1 (0.0%)	-
Congenital nevus	47 (0.5%)	47 (0.5%)
Dermatofibroma	845 (8.2%)	845 (8.2%)
Epidermal cyst	1,501 (14.6%)	1,501 (14.6%)
Epidermal nevus	26 (0.3%)	26 (0.3%)
Hemangioma	263 (2.6%)	263 (2.5%)
Juvenile xanthogranuloma	4 (0.0%)	-

Lentigo	67 (0.7%)	67 (0.6%)
Lymphangioma	15 (0.1%)	15 (0.1%)
Melanocytic nevus	1,441 (14.0%)	1,441 (14.0%)
Milia	8 (0.1%)	-
Mucocele	73 (0.7%)	73 (0.7%)
Mucosal melanotic macule	36 (0.4%)	36 (0.3%)
Neurofibroma	199 (1.9%)	199 (1.9%)
Nevus spilus	3 (0.0%)	-
Organoid nevus	62 (0.6%)	62 (0.6%)
Ota nevus	24 (0.2%)	24 (0.2%)
Porokeratosis	71 (0.7%)	71 (0.7%)
Poroma	64 (0.6%)	64 (0.6%)
Portwinestain	15 (0.1%)	15 (0.1%)
Pyogenic granuloma	162 (1.6%)	162 (1.6%)
Sebaceous hyperplasia	6 (0.1%)	-
Seborrheic keratosis	2,370 (23.1%)	2,370 (23.0%)
Skin tag	70 (0.7%)	70 (0.7%)
Spitz nevus	17 (0.2%)	-
Syringoma	103 (1.0%)	103 (1.0%)
Venous lake	101 (1.0%)	101 (1.0%)
Wart	636 (6.2%)	636 (6.2%)
Xanthelasma	18 (0.2%)	18 (0.2%)

The Severance validation dataset came from the Severance Hospital, Department of Dermatology and comprised both 34 benign and 9 malignant tumors.

The distribution of malignant tumors by anatomic location of the Severance Dataset A is as follows : head and neck 819 cases (7.9%), trunk 162 cases (1.6%), leg 153 cases (1.5%), arm 88 cases (0.8%). The distribution of benign tumors by anatomic location is as follows : head and neck 4,266 cases (40.9%), trunk 2,523 cases (24.2%), leg 1,433 cases (13.7%), arm 982 cases (9.4%).

Table 2. Sensitivity, Specificity, Positive Predictive Value, and Negative Predictive Value of the Algorithm at Two Predefined Cutoff Thresholds.

Disease	Classifier	Sensitivity (95% CI)	Specificity (95% CI)	PPV (95% CI)	NPV (95% CI)
All malignant tumors	Algorithm				
1,222 patients	High-Sensitivity Threshold	79.1 (76.9–81.4)	76.9 (76.1–77.8)	31.3 (30.3–32.3)	96.5 (96.2–96.9)
	High-Specificity Threshold	62.7 (59.9–65.5)	90.0 (89.4–90.6)	45.4 (43.7–47.3)	94.8 (94.4–95.2)
	Clinical Diagnosis				
	Top-1	70.2	95.6	68.1	96.0
	Top-2	84.9	86.0	44.6	97.7
	Top-3	88.1	83.8	41.9	98.1
Basal cell carcinoma	Algorithm				
643 patients	High-Sensitivity Threshold	81.3 (78.2–84.3)	76.9 (76.0–77.8)	19.8 (18.9–20.6)	98.3 (98.0–98.6)
	High-Specificity Threshold	66.6 (63.0–70.1)	90.0 (89.3–90.6)	31.7 (30.0–33.6)	97.5 (97.2–97.7)
	Clinical Diagnosis				
	Top-1	74.0	95.6	54.2	98.1
	Top-2	87.7	86.0	30.4	99.0
	Top-3	90.4	83.8	28.0	99.2
Squamous cell carcinoma	Algorithm				
158 patients	High-Sensitivity Threshold	84.2 (78.5–89.9)	76.9 (76.1–77.8)	5.9 (5.5–6.3)	99.7 (99.5–99.8)
	High-Specificity Threshold	70.9 (63.3–77.8)	90.0 (89.4–90.6)	10.8 (9.7–12.0)	99.5 (99.3–99.6)
	Clinical Diagnosis				
	Top-1	65.8	95.6	20.6	99.4
	Top-2	84.2	86.0	9.3	99.7
	Top-3	86.1	83.8	8.3	99.7
Malignant melanoma	Algorithm				
83 patients	High-Sensitivity Threshold	81.9 (73.5–90.4)	76.9 (76.0–77.8)	3.1 (2.8–3.4)	99.8 (99.7–99.9)
	High-Specificity Threshold	61.4 (50.6–72.3)	90.0 (89.4–90.6)	5.3 (4.3–6.1)	99.6 (99.5–99.7)
	Clinical Diagnosis				
	Top-1	68.7	95.6	12.4	99.7
	Top-2	84.3	86.0	5.1	99.8
	Top-3	89.2	83.8	4.7	99.9

Algorithm analyzed unprocessed images from 1,222 patients of malignant tumor and 9,204 patients of benign tumor (Severance Dataset A). The result of each malignant tumor was calculated with the patients with malignant tumor of interest and the 9,204 patients with benign tumor.

Table 3. Multiclass Task - AUC and Top Accuracies of the Algorithm compared with Human Experts with the 32 Skin Tumors of the Severance dataset

			Clinical Diagnosis			Algorithm			
No.	**Class Name**	**Image Number**	**Top-1 Accuracy**	**Top-2 Accuracy**	**Top-3 Accuracy**	**Top-1 Accuracy**	**Top-2 Accuracy**	**Top-3 Accuracy**	**AUC (95% CI)**
1	Actinic keratosis	784	68.8%	78.4%	80.2%	26.4%	42.1%	52.3%	0.925 (0.915–0.934)
2	Angiokeratoma	39	66.7%	69.2%	69.2%	46.2%	56.4%	64.1%	0.931 (0.891–0.968)
3	Basal cell carcinoma	643	64.5%	75.0%	77.3%	47.0%	59.7%	66.6%	0.915 (0.902–0.927)
4	Becker nevus	14	85.7%	85.7%	85.7%	42.9%	42.9%	50.0%	0.994 (0.982–1.000)
5	Blue nevus	115	71.3%	78.3%	79.1%	71.3%	82.6%	84.3%	0.967 (0.948–0.981)
6	Congenital nevus	47	68.1%	70.2%	70.2%	31.9%	57.4%	68.1%	0.940 (0.891–0.975)
7	Dermatofibroma	845	72.7%	78.9%	79.6%	71.6%	81.9%	86.3%	0.950 (0.942–0.958)
8	Epidermal cyst	1501	80.7%	86.2%	87.1%	56.0%	70.2%	77.5%	0.956 (0.951–0.961)
9	Epidermal nevus	26	53.8%	69.2%	69.2%	26.9%	26.9%	30.8%	0.907 (0.835–0.965)
10	Hemangioma	263	43.0%	50.6%	52.1%	30.8%	46.8%	57.4%	0.875 (0.852–0.898)
11	Intraepithelial carcinoma	255	43.1%	51.8%	54.9%	16.5%	28.6%	34.5%	0.888 (0.869–0.905)
12	Keratoacanthoma	15	66.7%	80.0%	80.0%	46.7%	80.0%	86.7%	0.990 (0.978–0.997)
13	Lentigo	67	43.3%	55.2%	55.2%	35.8%	47.8%	53.7%	0.870 (0.825–0.909)
14	Lymphangioma	15	13.3%	20.0%	20.0%	0.0%	0.0%	0.0%	0.676 (0.550–0.798)
15	Malignant melanoma	83	61.4%	77.1%	80.7%	39.8%	62.7%	66.3%	0.918 (0.888–0.945)
16	Melanocytic nevus	1441	71.3%	78.0%	78.5%	60.7%	76.3%	84.6%	0.914 (0.906–0.922)
17	Mucocele	73	84.9%	87.7%	89.0%	27.4%	45.2%	47.9%	0.985 (0.971–0.994)
18	Mucosal melanotic macule	36	69.4%	72.2%	72.2%	77.8%	86.1%	88.9%	0.997 (0.995–0.999)
19	Neurofibroma	199	51.8%	57.3%	57.8%	43.7%	57.3%	62.3%	0.943 (0.925–0.957)
20	Orgarnoid nevus	62	80.6%	88.7%	88.7%	62.9%	79.0%	82.3%	0.966 (0.930–0.989)
21	Ota nevus	24	79.2%	83.3%	83.3%	54.2%	66.7%	75.0%	0.999 (0.998–1.000)
22	Porokeratosis	71	77.5%	91.5%	91.5%	62.0%	73.2%	77.5%	0.967 (0.942–0.987)
23	Poroma	64	31.3%	40.6%	40.6%	4.7%	7.8%	9.4%	0.842 (0.787–0.889)
24	Portwine stain	15	66.7%	80.0%	80.0%	53.3%	60.0%	60.0%	0.907 (0.780–0.998)
25	Pyogenic granuloma	162	87.0%	92.0%	92.6%	65.4%	81.5%	88.9%	0.966 (0.945–0.981)
26	Seborrheic keratosis	2370	65.1%	78.4%	79.3%	48.5%	64.6%	72.2%	0.910 (0.904–0.916)
27	Skin tag	70	78.6%	87.1%	87.1%	14.3%	35.7%	42.9%	0.962 (0.945–0.977)
28	Squamous cell carcinoma	158	44.9%	69.6%	72.2%	28.5%	47.5%	56.3%	0.912 (0.889–0.933)
29	Syringoma	103	56.3%	62.1%	63.1%	6.8%	17.5%	27.2%	0.963 (0.942–0.981)
30	Venous lake	101	81.2%	86.1%	87.1%	40.6%	55.4%	65.3%	0.980 (0.961–0.993)
31	Wart	636	68.9%	83.0%	85.2%	49.4%	66.2%	74.4%	0.886 (0.875–0.898)
32	Xanthelasma	18	94.4%	100.0%	100.0%	72.2%	88.9%	88.9%	0.998 (0.995–1.000)
	Average	322±541	65.4±17.7%	73.9±16.6%	74.7±16.6%	42.6±20.7%	56.1±22.8%	61.9±22.9%	0.931±0.062

Algorithm analyzed the Severance Dataset B (39,721 images of 10,315 patients; 32 disorders).

The images analyzed were cropped around lesion of interest.

We calculated the AUC value of ROC curve in a one-versus-rest manner.

Table 4. Multiclass Task - AUC and Top Accuracies of the Algorithm with 10 Skin Tumors of the Edinburgh dataset

No.	Class Name	Image Number	Algorithm Top-1 Accuracy	Top-2 Accuracy	Top-3 Accuracy	AUC (95% CI)
1	Actinic keratosis	45	46.7%	75.6%	77.8%	0.956 (0.938–0.972)
2	Basal cell carcinoma	239	60.3%	72.4%	78.2%	0.940 (0.923–0.955)
3	Intraepithelial carcinoma	78	17.9%	33.3%	39.7%	0.889 (0.858–0.915)
4	Dermatofibroma	65	50.8%	66.2%	73.8%	0.962 (0.945–0.978)
5	Hemangioma	97	40.2%	55.7%	63.9%	0.886 (0.850–0.917)
6	Malignant melanoma	76	61.8%	78.9%	92.1%	0.942 (0.914–0.965)
7	Melanocytic nevus	331	79.8%	90.3%	94.0%	0.959 (0.945–0.971)
8	Pyogenic granuloma	24	62.5%	79.2%	87.5%	0.978 (0.962–0.991)
9	Seborrheic keratosis	257	68.5%	80.5%	87.2%	0.944 (0.927–0.960)
10	Squamous cell carcinoma	88	42.0%	76.1%	81.8%	0.932 (0.909–0.951)
	Average	130	53.0±17.4%	70.8±16.1%	77.6±16.1%	0.939±0.030

Algorithm analyzed 1,300 images of the Edinburgh dataset (https://licensing.edinburgh-innovations.ed.ac.uk/i/software/dermofit-image-library.html).

All the images of the Edinburgh dataset were cropped images of lesion of interest.

We calculated the AUC value of ROC curve in a one-versus-rest manner.

REFERENCES

1. Gulshan V, Peng L, Coram M, et al. Development and validation of a deep learning algorithm for detection of diabetic retinopathy in retinal fundus photographs. Jama 2016;316:2402-10.
2. Rajpurkar P, Irvin J, Ball RL, et al. Deep learning for chest radiograph diagnosis: A retrospective comparison of the CheXNeXt algorithm to practicing radiologists. PLoS medicine 2018;15:e1002686.
3. Chilamkurthy S, Ghosh R, Tanamala S, et al. Deep learning algorithms for detection of critical findings in head CT scans: a retrospective study. The Lancet 2018;392:2388-96.
4. Esteva A, Kuprel B, Novoa RA, et al. Dermatologist-level classification of skin cancer with deep neural networks. Nature 2017;542:115-8.
5. Han SS, Kim MS, Lim W, Park GH, Park I, Chang SE. Classification of the Clinical Images for Benign and Malignant Cutaneous Tumors Using a Deep Learning Algorithm. Journal of Investigative Dermatology 2018.
6. Fujisawa Y, Otomo Y, Ogata Y, et al. Deep learning-based, computer-aided classifier developed with a small dataset of clinical images surpasses board-certified dermatologists in skin tumor diagnosis. British Journal of Dermatology 2018.
7. Tschandl P, Rosendahl C, Akay BN, et al. Expert-Level Diagnosis of Nonpigmented Skin Cancer by Combined Convolutional Neural Networks. JAMA dermatology 2018.
8. Cho S, Sun S, Mun J, et al. Dermatologist-level classification of malignant lip diseases using a deep convolutional neural network. British Journal of Dermatology 2019.
9. Han SS, Moon IJ, Lim W, et al. Keratinocytic Skin Cancer Detection on the Face Using Region-Based Convolutional Neural Network. JAMA dermatology 2019.
10. Haenssle H, Fink C, Schneiderbauer R, et al. Man against machine: diagnostic performance of a deep learning convolutional neural network for dermoscopic melanoma recognition in comparison to 58 dermatologists. Annals of Oncology 2018.
11. Brinker TJ, Hekler A, Enk AH, et al. A convolutional neural network trained with dermoscopic images performed on par with 145 dermatologists in a clinical melanoma image classification task. European Journal of Cancer 2019;111:148-54.
12. Maron RC, Weichenthal M, Utikal JS, et al. Systematic outperformance of 112 dermatologists in multiclass skin cancer image classification by convolutional neural networks. European Journal of Cancer 2019;119:57-65.
13. Tschandl P, Codella N, Akay BN, et al. Comparison of the accuracy of human readers versus machine-learning algorithms for pigmented skin lesion classification: an open, web-based, international, diagnostic study. The Lancet Oncology 2019.

14. Topol EJ. High-performance medicine: the convergence of human and artificial intelligence. Nature medicine 2019;25:44.
15. Silver D, Huang A, Maddison CJ, et al. Mastering the game of Go with deep neural networks and tree search. Nature 2016;529:484.
16. Kendall A, Gal Y. What uncertainties do we need in bayesian deep learning for computer vision? Advances in neural information processing systems; 2017. p. 5574-84.
17. Tschandl P. Problems and Potentials of Automated Object Detection for Skin Cancer Recognition. JAMA dermatology 2019.
18. Brinker TJ, Hekler A, Utikal JS, et al. Skin cancer classification using convolutional neural networks: systematic review. Journal of medical Internet research 2018;20:e11936.
19. Liu X, Faes L, Kale AU, et al. A comparison of deep learning performance against health-care professionals in detecting diseases from medical imaging: a systematic review and meta-analysis. The Lancet Digital Health 2019;1:e271-e97.
20. Chuchu N, Takwoingi Y, Dinnes J, et al. Cochrane Skin Cancer Diagnostic Test Accuracy Group. Smartphone applications for triaging adults with skin lesions that are suspicious for melanoma. status and date: New, published in 2018.
21. Xiong M, Pfau J, Young AT, Wei ML. Artificial Intelligence in Teledermatology. Current Dermatology Reports 2019;8:85-90.
22. Navarrete-Dechent C, Dusza SW, Liopyris K, Marghoob AA, Halpern AC, Marchetti MA. Automated Dermatological Diagnosis: Hype or Reality? Journal of Investigative Dermatology 2018.
23. Winkler JK, Fink C, Toberer F, et al. Association between surgical skin markings in dermoscopic images and diagnostic performance of a deep learning convolutional neural network for melanoma recognition. JAMA dermatology 2019.
24. Nisbet R, Elder J, Miner G. Handbook of statistical analysis and data mining applications: Academic Press; 2009.
25. Parikh RB, Teeple S, Navathe AS. Addressing Bias in Artificial Intelligence in Health Care. JAMA 2019.
26. Narla A, Kuprel B, Sarin K, Novoa R, Ko J. Automated classification of skin lesions: from pixels to practice. Journal of Investigative Dermatology 2018;138:2108-10.
27. Pacheco AG, Krohling RA. The impact of patient clinical information on automated skin cancer detection. arXiv preprint arXiv:190912912 2019.
28. Yap J, Yolland W, Tschandl P. Multimodal skin lesion classification using deep learning. Experimental dermatology 2018;27:1261-7.
29. Liu Y, Jain A, Eng C, et al. A deep learning system for differential diagnosis of skin diseases. arXiv preprint arXiv:190905382 2019.

30. Dodge S, Karam L. A study and comparison of human and deep learning recognition performance under visual distortions. 2017 26th international conference on computer communication and networks (ICCCN); 2017: IEEE. p. 1-7.

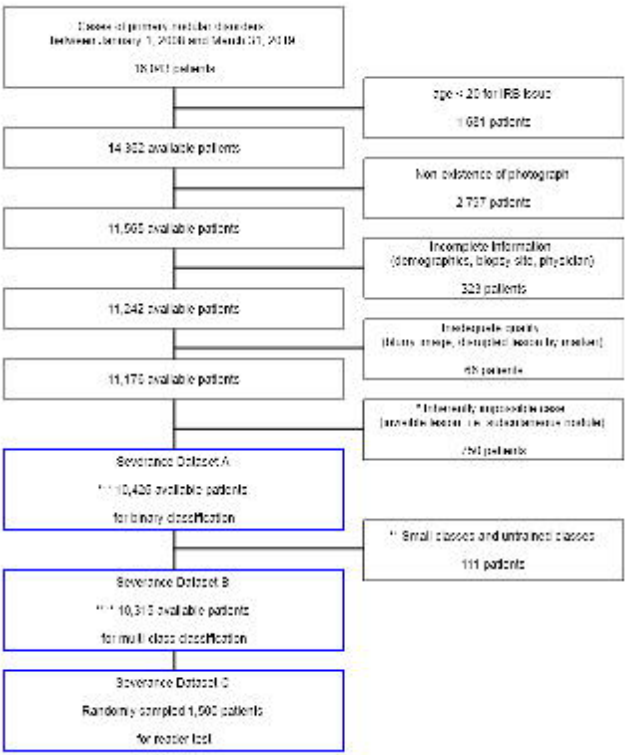
Classes of primary modular disorders
between January 1, 2008 and March 31, 2019
18,000 patients
age < 20 for IRB issue
1,681 patients
14,362 available patients
Non existence of photograph
2,737 patients
11,565 available patients
Incomplete information
(demographics, biopsy site, physician)
323 patients
11,242 available patients
Inadequate quality
(blurry image, disrupted tissue by marker)
68 patients
11,176 available patients
* Intensively unpossible cases
(unreliable lesson in subcutaneous nodule)
750 patients
Severance Dataset A
** 10,426 available patients
for binary classification
** Small classes and untrained classes
111 patients
Severance Dataset B
*** 10,315 available patients
for multi class classification
Severance Dataset C
Randomly sampled 1,500 patients
for reader test

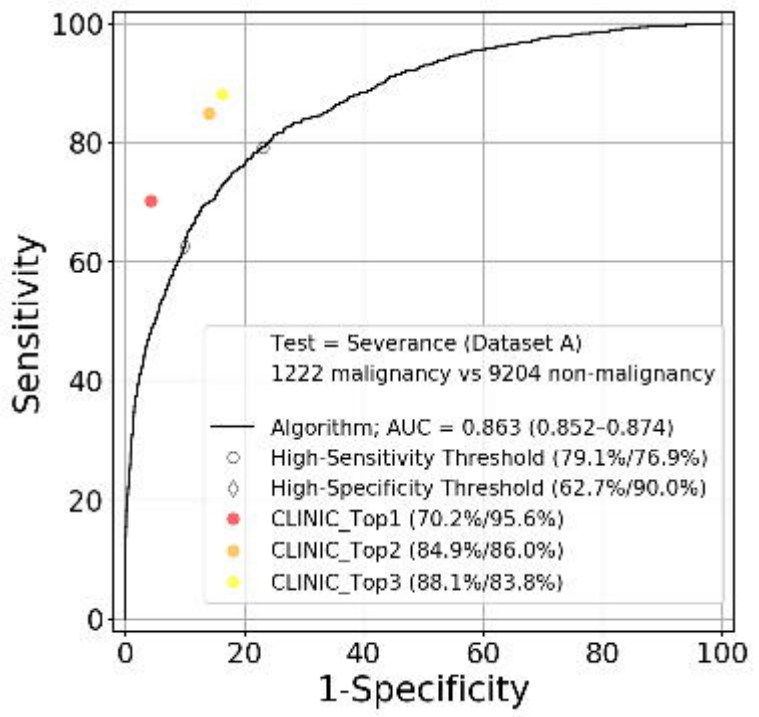
Test = Severance (Dataset A)
1222 malignancy vs 9204 non-malignancy
Algorithm; AUC = 0.863 (0.852–0.874)
High-Sensitivity Threshold (79.1%/76.9%)
High-Specificity Threshold (62.7%/90.0%)
CLINIC_Top1 (70.2%/95.6%)
CLINIC_Top2 (84.9%/86.0%)
CLINIC_Top3 (88.1%/83.8%)
Sensitivity
1-Specificity
0
20
40
60
80
100

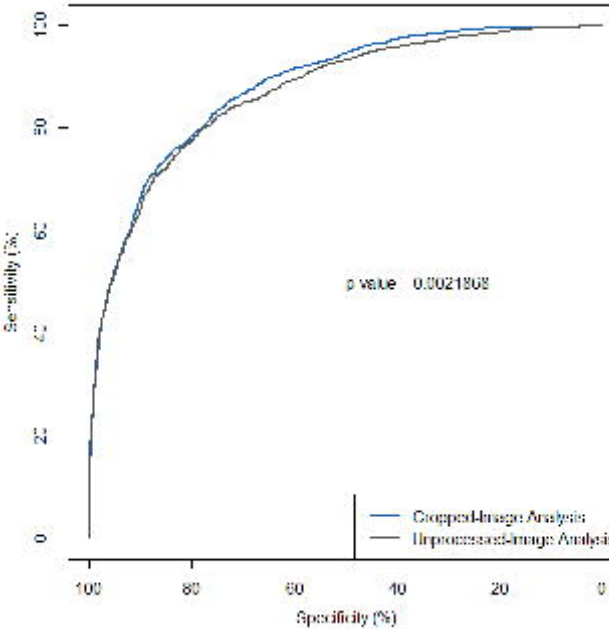
p value 0.0021808
Cropped-Image Analysis
Unprocessed-Image Analysis
Sensitivity (%)
Specificity (%)
100
80
60
40
20
0

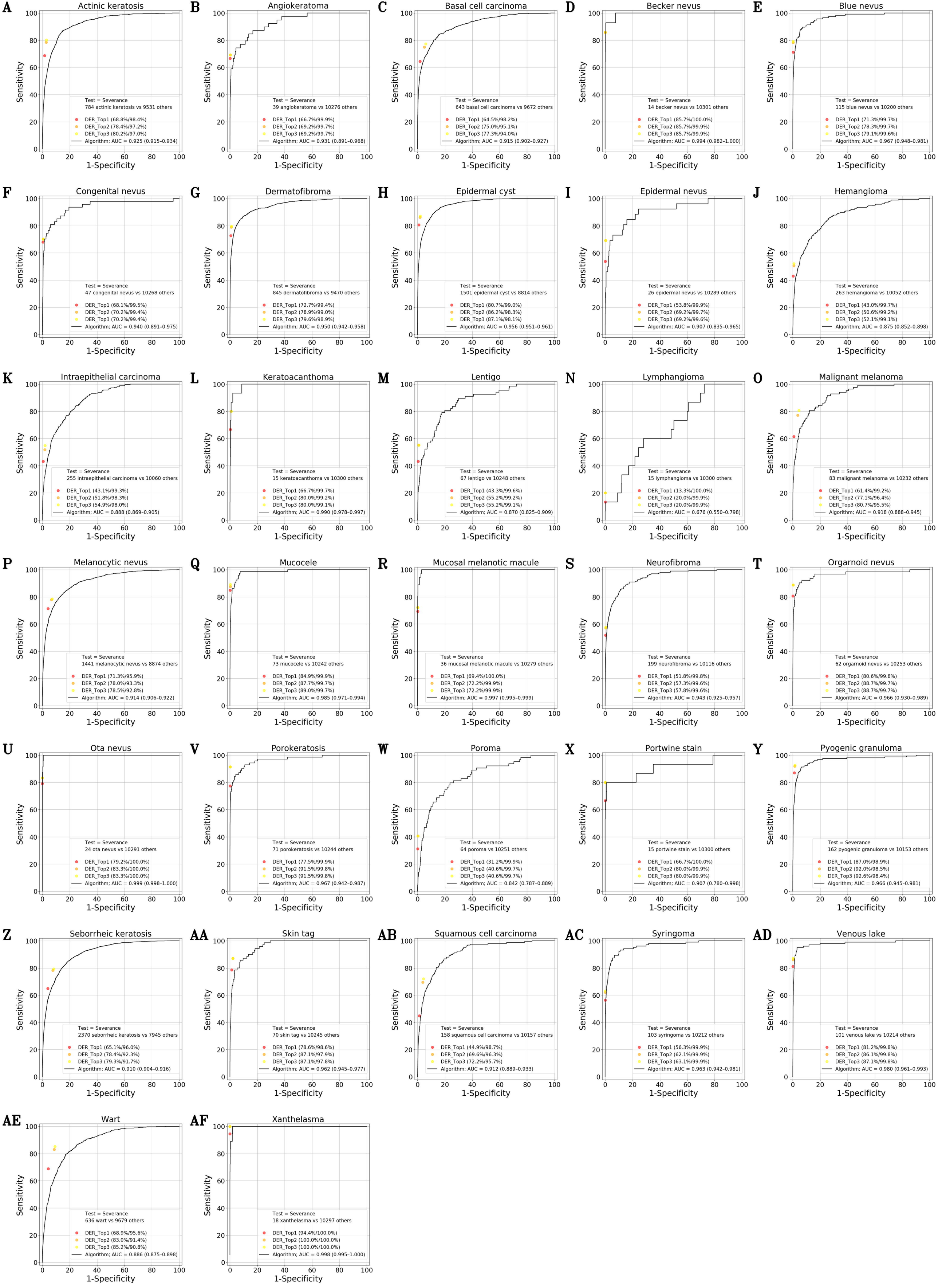
A
Actinic keratosis
Test = Severance
784 actinic keratosis vs 9531 others
DER_Top1 (68.8%/98.4%)
DER_Top2 (78.4%/97.2%)
DER_Top3 (80.2%/97.0%)
Algorithm; AUC = 0.925 (0.915–0.934)
B
Angiokeratoma
Test = Severance
39 angiokeratoma vs 10276 others
DER_Top1 (66.7%/99.9%)
DER_Top2 (69.2%/99.7%)
DER_Top3 (69.2%/99.7%)
Algorithm; AUC = 0.931 (0.891–0.968)
C
Basal cell carcinoma
Test = Severance
643 basal cell carcinoma vs 9672 others
DER_Top1 (64.5%/98.2%)
DER_Top2 (75.0%/95.1%)
DER_Top3 (77.3%/94.0%)
Algorithm; AUC = 0.915 (0.902–0.927)
D
Becker nevus
Test = Severance
14 becker nevus vs 10301 others
DER_Top1 (85.7%/100.0%)
DER_Top2 (85.7%/99.9%)
DER_Top3 (85.7%/99.9%)
Algorithm; AUC = 0.994 (0.982–1.000)
E
Blue nevus
Test = Severance
115 blue nevus vs 10200 others
DER_Top1 (71.3%/99.7%)
DER_Top2 (78.3%/99.7%)
DER_Top3 (79.1%/99.6%)
Algorithm; AUC = 0.967 (0.948–0.981)
F
Congenital nevus
Test = Severance
47 congenital nevus vs 10268 others
DER_Top1 (68.1%/99.5%)
DER_Top2 (70.2%/99.4%)
DER_Top3 (70.2%/99.4%)
Algorithm; AUC = 0.940 (0.891–0.975)
G
Dermatofibroma
Test = Severance
845 dermatofibroma vs 9470 others
DER_Top1 (72.7%/99.4%)
DER_Top2 (78.9%/99.0%)
DER_Top3 (79.6%/98.9%)
Algorithm; AUC = 0.950 (0.942–0.958)
H
Epidermal cyst
Test = Severance
1501 epidermal cyst vs 8814 others
DER_Top1 (80.7%/99.0%)
DER_Top2 (86.2%/98.3%)
DER_Top3 (87.1%/98.1%)
Algorithm; AUC = 0.956 (0.951–0.961)
I
Epidermal nevus
Test = Severance
26 epidermal nevus vs 10289 others
DER_Top1 (53.8%/99.9%)
DER_Top2 (69.2%/99.7%)
DER_Top3 (69.2%/99.6%)
Algorithm; AUC = 0.907 (0.835–0.965)
J
Hemangioma
Test = Severance
263 hemangioma vs 10052 others
DER_Top1 (43.0%/99.7%)
DER_Top2 (50.6%/99.2%)
DER_Top3 (52.1%/99.1%)
Algorithm; AUC = 0.875 (0.852–0.898)
K
Intraepithelial carcinoma
Test = Severance
255 intraepithelial carcinoma vs 10060 others
DER_Top1 (43.1%/99.3%)
DER_Top2 (51.8%/98.3%)
DER_Top3 (54.9%/98.0%)
Algorithm; AUC = 0.888 (0.869–0.905)
L
Keratoacanthoma
Test = Severance
15 keratoacanthoma vs 10300 others
DER_Top1 (66.7%/99.7%)
DER_Top2 (80.0%/99.2%)
DER_Top3 (80.0%/99.1%)
Algorithm; AUC = 0.990 (0.978–0.997)
M
Lentigo
Test = Severance
67 lentigo vs 10248 others
DER_Top1 (43.3%/99.6%)
DER_Top2 (55.2%/99.2%)
DER_Top3 (55.2%/99.1%)
Algorithm; AUC = 0.870 (0.825–0.909)
N
Lymphangioma
Test = Severance
15 lymphangioma vs 10300 others
DER_Top1 (13.3%/100.0%)
DER_Top2 (20.0%/99.9%)
DER_Top3 (20.0%/99.9%)
Algorithm; AUC = 0.676 (0.550–0.798)
O
Malignant melanoma
Test = Severance
83 malignant melanoma vs 10232 others
DER_Top1 (61.4%/99.2%)
DER_Top2 (77.1%/96.4%)
DER_Top3 (80.7%/95.5%)
Algorithm; AUC = 0.918 (0.888–0.945)
P
Melanocytic nevus
Test = Severance
1441 melanocytic nevus vs 8874 others
DER_Top1 (71.3%/95.9%)
DER_Top2 (78.0%/93.3%)
DER_Top3 (78.5%/92.8%)
Algorithm; AUC = 0.914 (0.906–0.922)
Q
Mucocele
Test = Severance
73 mucocele vs 10242 others
DER_Top1 (84.9%/99.9%)
DER_Top2 (87.7%/99.7%)
DER_Top3 (89.0%/99.7%)
Algorithm; AUC = 0.985 (0.971–0.994)
R
Mucosal melanotic macule
Test = Severance
36 mucosal melanotic macule vs 10279 others
DER_Top1 (69.4%/100.0%)
DER_Top2 (72.2%/99.9%)
DER_Top3 (72.2%/99.9%)
Algorithm; AUC = 0.997 (0.995–0.999)
S
Neurofibroma
Test = Severance
199 neurofibroma vs 10116 others
DER_Top1 (51.8%/99.8%)
DER_Top2 (57.3%/99.6%)
DER_Top3 (57.8%/99.6%)
Algorithm; AUC = 0.943 (0.925–0.957)
T
Orgarnoid nevus
Test = Severance
62 orgarnoid nevus vs 10253 others
DER_Top1 (80.6%/99.8%)
DER_Top2 (88.7%/99.7%)
DER_Top3 (88.7%/99.7%)
Algorithm; AUC = 0.966 (0.930–0.989)
U
Ota nevus
Test = Severance
24 ota nevus vs 10291 others
DER_Top1 (79.2%/100.0%)
DER_Top2 (83.3%/100.0%)
DER_Top3 (83.3%/100.0%)
Algorithm; AUC = 0.999 (0.998–1.000)
V
Porokeratosis
Test = Severance
71 porokeratosis vs 10244 others
DER_Top1 (77.5%/99.9%)
DER_Top2 (91.5%/99.8%)
DER_Top3 (91.5%/99.8%)
Algorithm; AUC = 0.967 (0.942–0.987)
W
Poroma
Test = Severance
64 poroma vs 10251 others
DER_Top1 (31.2%/99.9%)
DER_Top2 (40.6%/99.7%)
DER_Top3 (40.6%/99.7%)
Algorithm; AUC = 0.842 (0.787–0.889)
X
Portwine stain
Test = Severance
15 portwine stain vs 10300 others
DER_Top1 (66.7%/100.0%)
DER_Top2 (80.0%/99.9%)
DER_Top3 (80.0%/99.9%)
Algorithm; AUC = 0.907 (0.780–0.998)
Y
Pyogenic granuloma
Test = Severance
162 pyogenic granuloma vs 10153 others
DER_Top1 (87.0%/98.9%)
DER_Top2 (92.0%/98.5%)
DER_Top3 (92.6%/98.4%)
Algorithm; AUC = 0.966 (0.945–0.981)
Z
Seborrheic keratosis
Test = Severance
2370 seborrheic keratosis vs 7945 others
DER_Top1 (65.1%/96.0%)
DER_Top2 (78.4%/92.3%)
DER_Top3 (79.3%/91.7%)
Algorithm; AUC = 0.910 (0.904–0.916)
AA
Skin tag
Test = Severance
70 skin tag vs 10245 others
DER_Top1 (78.6%/98.6%)
DER_Top2 (87.1%/97.9%)
DER_Top3 (87.1%/97.8%)
Algorithm; AUC = 0.962 (0.945–0.977)
AB
Squamous cell carcinoma
Test = Severance
158 squamous cell carcinoma vs 10157 others
DER_Top1 (44.9%/98.7%)
DER_Top2 (69.6%/96.3%)
DER_Top3 (72.2%/95.7%)
Algorithm; AUC = 0.912 (0.889–0.933)
AC
Syringoma
Test = Severance
103 syringoma vs 10212 others
DER_Top1 (56.3%/99.9%)
DER_Top2 (62.1%/99.9%)
DER_Top3 (63.1%/99.9%)
Algorithm; AUC = 0.963 (0.942–0.981)
AD
Venous lake
Test = Severance
101 venous lake vs 10214 others
DER_Top1 (81.2%/99.8%)
DER_Top2 (86.1%/99.8%)
DER_Top3 (87.1%/99.8%)
Algorithm; AUC = 0.980 (0.961–0.993)
AE
Wart
Test = Severance
636 wart vs 9679 others
DER_Top1 (68.9%/95.6%)
DER_Top2 (83.0%/91.4%)
DER_Top3 (85.2%/90.8%)
Algorithm; AUC = 0.886 (0.875–0.898)
AF
Xanthelasma
Test = Severance
18 xanthelasma vs 10297 others
DER_Top1 (94.4%/100.0%)
DER_Top2 (100.0%/100.0%)
DER_Top3 (100.0%/100.0%)
Algorithm; AUC = 0.998 (0.995–1.000)
Sensitivity
1-Specificity

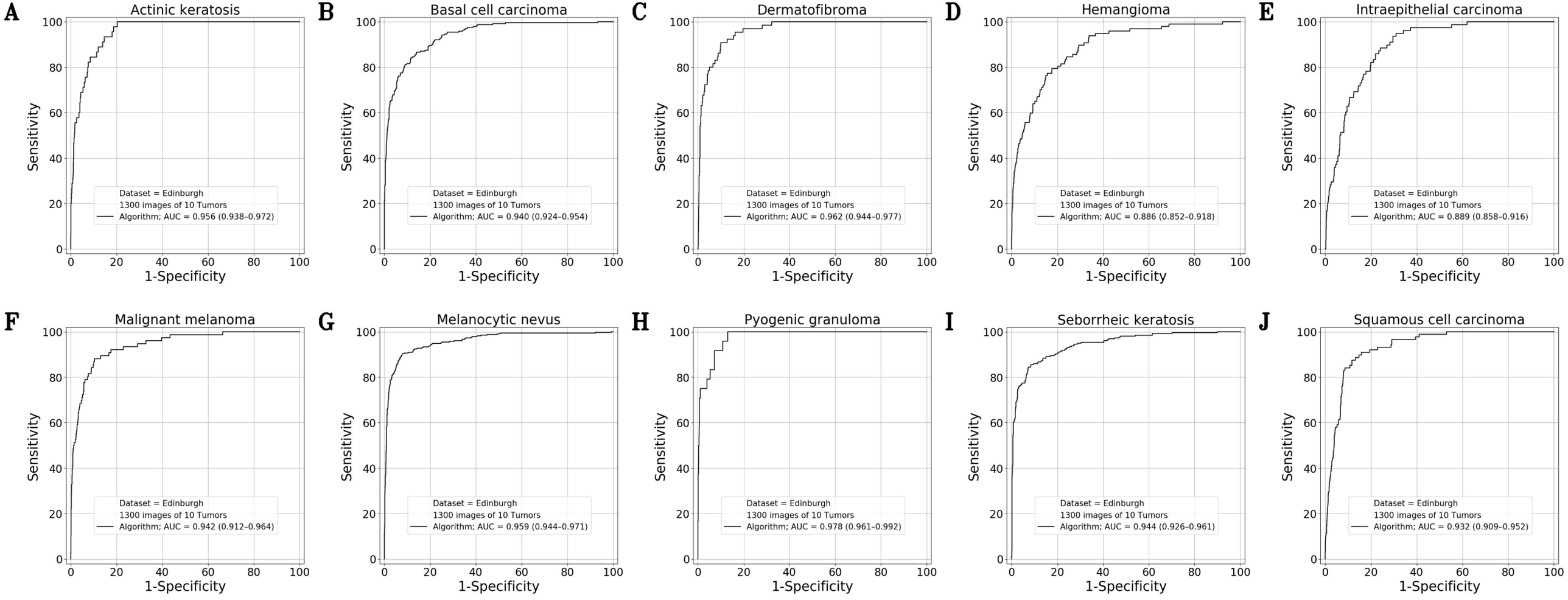
A
Actinic keratosis
Dataset = Edinburgh
1300 images of 10 Tumors
Algorithm; AUC = 0.956 (0.938–0.972)
B
Basal cell carcinoma
Dataset = Edinburgh
1300 images of 10 Tumors
Algorithm; AUC = 0.940 (0.924–0.954)
C
Dermatofibroma
Dataset = Edinburgh
1300 images of 10 Tumors
Algorithm; AUC = 0.962 (0.944–0.977)
D
Hemangioma
Dataset = Edinburgh
1300 images of 10 Tumors
Algorithm; AUC = 0.886 (0.852–0.918)
E
Intraepithelial carcinoma
Dataset = Edinburgh
1300 images of 10 Tumors
Algorithm; AUC = 0.889 (0.858–0.916)
F
Malignant melanoma
Dataset = Edinburgh
1300 images of 10 Tumors
Algorithm; AUC = 0.942 (0.912–0.964)
G
Melanocytic nevus
Dataset = Edinburgh
1300 images of 10 Tumors
Algorithm; AUC = 0.959 (0.944–0.971)
H
Pyogenic granuloma
Dataset = Edinburgh
1300 images of 10 Tumors
Algorithm; AUC = 0.978 (0.961–0.992)
I
Seborrheic keratosis
Dataset = Edinburgh
1300 images of 10 Tumors
Algorithm; AUC = 0.944 (0.926–0.961)
J
Squamous cell carcinoma
Dataset = Edinburgh
1300 images of 10 Tumors
Algorithm; AUC = 0.932 (0.909–0.952)
Sensitivity
1-Specificity
0
20
40
60
80
100